Langmuir

Article

pubs.acs.org/Langmuir

Surface Pressure and Microstructure of Carbon Nanotubes at an Air−Water Interface

Sahil R. Vora,[†] Brice Bognet,[‡,§] Huseini S. Patanwala,[‡] Francisco Chinesta,[§] and Anson W. K. Ma*[,†,‡]

[†]Department of Chemical and Biomolecular Engineering, and [‡]Polymer Program, Institute of Materials Science, University of Connecticut, Storrs, Connecticut 06269, United States

[§]GeM UMR CNRS-Centrale Nantes, 1 rue de la Noë, F-44300 Nantes, France

Supporting Information

ABSTRACT: This article reports the surface pressure and microstructure of two different types of carbon nanotubes (CNTs) at an air−water interface; namely, as-produced CNTs (nf-CNTs) and CNTs functionalized with carboxyl groups (f-CNTs). Both types of CNTs formed 3D aggregates upon compression using a Langmuir−Pockels trough. However, f-CNTs showed a lower degree of aggregation compared with that of nf-CNTs. This is attributed to the deprotonation of the carboxyl groups within the water subphase, leading to additional electrostatic repulsion between f-CNTs. For the same initial amount of CNTs spread onto the interface, the actual coverage of f-CNTs was higher than that of nf-CNTs at a given trough area. At high compression, f-CNTs formed aligned CNT domains at the interface. These 2D domains resembled 3D liquid−crystalline structures formed by excluded volume interactions. The denser packing and orientational ordering of f-CNTs also contributed to a compressional modulus higher than that of nf-CNTs, as calculated from the surface pressure isotherms. A Volmer equation of state was applied to model the measured surface pressure containing both thermodynamic and mechanical contributions. The Volmer model, however, did not consider the loss of CNTs from the interface due to 3D aggregation and consequently overestimated the surface pressure at high compression. The actual coverage of CNT during compression was back calculated from the model and was in agreement with the value obtained independently from optical micrographs. The findings of this work may have a broader impact on understanding the assembly and collective behavior of rod-like particles with a high aspect ratio at an air−water interface.

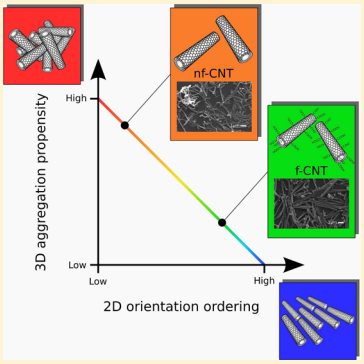

INTRODUCTION

It has been known for more than a hundred years that particles of appropriate size and wettability adsorb at the gas−liquid or liquid−liquid interface, consequently lowering the interfacial energy of the system.[1−4] The particles also form armor that protects the droplets or bubbles from coalescing. Particle-stabilized emulsions are commonly referred to as "Pickering emulsions," although the phenomenon was first noted by Ramsden[1] and a few years later by Pickering.[2] In recent years, there has been a resurgent interest in using particles to stabilize foams and emulsions, thereby improving the shelf lives of pharmaceutical, agricultural, and personal care products. New types of Pickering−Ramsden emulsions may also open up novel applications such as enhanced oil recovery[5,6] and oil spill cleanups.[7,8]

The assembly of particles at the interface is modulated by electrostatic interactions and/or lateral capillary interactions. Early description of interface-driven assembly can be found in the seminal work of Pieranski[9] in 1980. Pieranski showed that negatively charged polystyrene spheres with a diameter of 245 nm assemble into a 2-D triangular lattice at the air−water interface. Their studies suggested that the electrostatic interactions between nanoparticles at the interface involve Coulombic interactions as well as dipole−dipole interactions caused by the asymmetric counterion distribution along the interface.[10−12] In addition to electrostatic interactions, undulation of the contact line may occur, leading to lateral capillary interactions. However, the exact origin for lateral capillary interactions is still debatable[13,14] and may vary from one system to another. Gravity,[15] particle shape,[16,17] and surface roughness,[18] electric-field induced dipping effect,[19] and external electric field[20] have all been proposed as possible origins. Excellent reviews on this topic have been written by Binks[3] and Botto et al.[21]

In terms of the effect of particle shape, Basavaraj et al.[22] studied the optical microstructure and surface pressure of both polystyrene spheres and ellipsoidal particles prepared by thermo-mechanical stretching. Their studies showed that ellipsoidal particles have less pronounced phase transitions relative to spheres. They also noticed the formation of "flippers," wherein the ellipsoidal particles assumed an orientation perpendicular to the air−water interface (i.e., parallel to the surface norm of the air−water interface). However, the exact origin is not entirely clear. More recently, Imperiali et al.[23] studied the structure and mechanical properties of graphene oxide (GO) sheets at an air−water

Received: December 19, 2014
Revised: April 1, 2015
Published: April 6, 2015

DOI: 10.1021/la504934x
Langmuir 2015, 31, 4663−4672

interface. The authors demonstrated that monolayer GO sheets at the interface formed an elastic, compact layer upon compression, which was then deposited on a substrate and chemically reduced to graphene.

Most existing studies focus on micron-sized particles with only a number of exceptions.[4,13,23−25] Thermal fluctuations would become increasingly important as the size of the particles decreases, further complicating the physics. Additionally, the aspect ratio, or the length-to-diameter ratio, of mechanically stretched ellipsoidal particles is typically less than 10. This article aims to investigate the assembly, surface pressure, and mechanical response of an air−water interface decorated with carbon nanotubes (CNTs) having a diameter on the order of 100 nm and an aspect ratio exceeding 40. Two types of CNTs with similar length distribution but different surface chemistry have been studied and contrasted. The goal to is to investigate the effects of CNT−CNT interactions and hydrophilicity on their collective behavior at the interface upon compression. Microstructure studies of this work revealed 3D aggregation and 2D orientational ordering of CNTs at an air−water interface. A new modified Volmer model is proposed based on the microstructure and surface pressure data.

EXPERIMENTAL METHODS

Materials. CNTs in this study were obtained from Sigma-Aldrich (Cat# 659258, Lot# MKBG9911V) and used without any further purification. The CNTs were multiwalled carbon nanotubes produced using the chemical vapor deposition (CVD) method. They have a diameter of ca. 110 nm and about 40 layers. The as-received CNTs are nonfunctionalized and will be referred to as "nf-CNTs." Carboxyl-functionalized carbon nanotubes (f-CNTs) were prepared by sonicating the nf-CNTs in a mixture of 3:1 sulfuric acid (98%; Fisher) and nitric acid (70%; Sigma-Aldrich) at a bath temperature of 50 °C (Branson sonicator).[26,27] The f-CNTs were recovered from the reactive acid mixture by vacuum filtration (10 μm polytetrafluoroethylene (PTFE) membrane, Millipore). Copious amounts of water were used for washing until the filtrate reached a pH of 6.5. The sample was then freeze-dried at −25 °C (Labconco FreeZone^6) for 72 h. Raman spectroscopy (Renishaw System 2000; 514 nm) was carried out on both the nf-CNTs and f-CNTs. The ratio of the D-band to G-band for nf-CNTs is ∼0.17, indicating the as-received CNTs are rather defect-free.[28] After functionalization, this ratio increased from 0.17 to 0.48 as the sp^2 carbon was converted to sp^3 carbon (Supporting Information, Figure S1).

CNT Length Characterization and Zeta Potential Measurements. For length characterization, CNTs were first dispersed in chloroform by sonication, dried, and resuspended in water, and then deposited onto a glass slide through water evaporation.[29] Scanning electron microscopy (SEM; JEOL 6335 field emission SEM) was carried out after sputtering a thin layer (3−5 nm) of gold and palladium onto the specimen. The length and diameter distributions of both nf-CNTs and f-CNTs were characterized using ImageJ. Surprisingly, no noticeable reduction in length was observed for f-CNTs, possibly because of the relatively low defect density and large number of walls (∼40) of the CNTs used in this study. The average length for both nf-CNT and f-CNT is 2.6 μm. From the length distribution data, the polydispersity index (PDI), defined as the ratio of weight-average length divided by the number-average length, was estimated to be 1.335 and 1.240 for the nf-CNTs and the f-CNTs, respectively. Likewise, the PDI for diameter distribution was calculated to be 1.077 and 1.089, for nf-CNTs, and f-CNTs (Supporting Information: Figures S2 and S3). Malvern Zetasizer ZS90 was used to measure the zeta potential of f-CNTs dispersed in deionized water.

Spreading Protocol and Surface Pressure Measurements. To prepare a spreading dispersion, dry powders of nf-CNT or f-CNTs were first dispersed in chloroform by sonication (Branson 450 Digital Sonifier; 2 h; 20% amplitude) at an initial concentration of 0.2 mg/mL. Chloroform was used as a dispersant given its immiscibility with water and ability to disperse CNTs. To remove large CNT aggregates, the dispersions were then centrifuged (Thermo Scientific Clinifuge, 3000 rpm, ∼500g; 10 min) or left undisturbed overnight. The actual concentration of the supernatant was calibrated by measuring the absorbance (Shimadzu, UVmini-1240 UV−vis spectrophotometer) at a wavelength of 500 nm. The detailed procedure and calibration curves are given in Supporting Information (Figure S4). The supernatant of the CNT dispersions did not show any optically resolvable aggregates. The CNT supernatant was then added dropwise onto an air−water interface using a 500-μL syringe over the course of 3 h until the desired CNT coverage was reached. The deionized water used was produced by a Millipore (Milli-Q) system with resistivity >18 MΩ. Because of the higher density of chloroform relative to water, the spreading dispersion was added slowly to avoid the formation of large chloroform drops, which would sink to the bottom of the trough. The chloroform spread onto the interface was allowed to evaporate before any actual surface pressure measurements. To rule out any surface pressure contribution from chloroform, a control experiment was carried out by spreading 12.5 mL of chloroform onto the air−water interface, in the absence of CNTs. The surface pressure remained zero for five cycles of compression and expansion.

The surface pressure was measured at room temperature (25 °C) using a microbalance and a Wilhelmy plate oriented perpendicular to the interface and parallel to the barriers. Wilhelmy plates made of surface-treated platinum and paper were tested. No significant difference in the surface pressure was recorded, although the paper-based plate consistently showed a slightly higher surface pressure due to the capillary action and water uptake (Supporting Information: Figure S5). As a result, a platinum-based Wilhelmy plate was used for all the studies reported in this article. The minimum compression area for the current setup (KN 3005 Langmuir−Pockels trough) is 23 cm^2. A higher CNT coverage can be achieved by increasing the initial amount of CNT spread onto the interface. During compression cycles, Derlin barriers moved at a rate of 5 mm/min (trough width = 146.7 mm). Previous studies showed that the measured surface pressure values may depend on the orientation of the Wilhelmy plate relative to the barriers as well as the compression rate.[30,31] These factors will be further investigated and reported in a future paper. Preliminary data on the effect of compression rate are included in Supporting Information (Figure S6). Although Wilhelmy plate is commonly used to measure the surface pressure of particle-laden interfaces,[32−34] the local CNT concentration close to the Wilhelmy plate is likely to be different from the rest of the interface due to local curvature, which is known to modify the spatial and orientational distribution of rod-like particles[16] and in turn affects the surface pressure readings.

In-Situ Optical Microscopy. The Langmuir−Pockels trough used in this study has a sapphire window at the center of the trough. Optical micrographs were captured by mounting the entire trough onto an upright bright-field optical microscope (Olympus BZ50; 5× magnification objective). Videos were recorded at a frame rate of 2 fps (iDS UI-3360CP-C-HQ) during the compression/expansion cycles for different trough areas.

Langmuir−Schaefer Deposition. Langmuir−Schaefer deposition was used to prepare thin films for optical and electron microscopy. In this method, a 20 mm × 20 mm glass coverslip was held horizontally above the interface using a suction cup. The glass substrate was then lowered at a speed of 5 mm/min until it made contact with the CNT-decorated interface. After the deposition, the substrate was removed form the interface at the same speed, and residue water was removed by drying the sample at 75 °C for 12 h in an oven. SEM on deposited films was performed to complement in situ optical microscopy, which is incapable of resolving individual CNTs due to the diffraction limit. As in length characterization, the sample was coated with a thin layer (3−5 nm) of palladium and gold to avoid charging during SEM. Although extra caution was exercised during deposition, the CNT arrangement may have been modified as the CNTs at the air−water interface were transferred onto an air−solid interface.

Contact Angle. As pointed out by Binks et al.,[3] measuring the contact angle of submicron particles always proves to be challenging.

DOI: 10.1021/la504934x
Langmuir 2015, 31, 4663−4672

The "gel trapping" method proposed by Paunov[35] was used to investigate the apparent contact angle of nf-CNTs and f-CNTs at the air−water interface. First, 2% (w/w) gellan gum (Sigma-Aldrich, Cat. No. P8169, Lot No. 011M0119 V) was dispersed in water, and the solution was heated to 95 °C to dissolve the gellan gum. No noticeable change in surface tension was observed after the addition of the gellan gum. The solution was then dispensed into a beaker with the temperature maintained at 50 °C using a hot plate. The CNTs were then spread onto the surface, and the solution was cooled down to room temperature using an ice bath. The beaker was covered and left undisturbed for 30 min to allow the gel to set. Polydimethylsiloxane (PDMS) elastomer (Sylgard 184) was prepared by mixing the PDMS with the curing agent in a 10:1 ratio, followed by degassing in the centrifuge at 2000 rpm to obtain a clear, bubble-free liquid. Soon after centrifugation, the liquid elastomer was poured over the gelled water and left to cure for 48 h at room temperature. The cross-linked elastomer was peeled off the gel surface and immersed in a water bath at 95 °C for 2 min to dissolve any residual gellan on the surface. To avoid covering the features of CNTs given their relative small diameter (ca. 110 nm), atomic force microscopy (AFM) was used instead of SEM, which requires the deposition of a conductive layer to prevent charging. AFM was carried out in tapping mode (Asylum Research MFP-3D AFM with an integrated Nikon TE-2000 inverted optical microscope, Santa Barbara, Sunnyvale, CA). Silicon nitride (Si_3N_4) probes (Microlever, Park Science Instruments, Sunnyvale, CA) were used with a pyramidal tip (radius of curvature: ∼50 nm) and a nominal spring constant of ∼0.06 N/m. The lever spring constant was calibrated before each measurement by the thermal noise method. The height obtained from the AFM images was used to estimate the position of the CNTs at the interface.

EXPERIMENTAL RESULTS AND DISCUSSION

Successive Compression Cycles and Formation of 3D CNT Aggregates. Figure 1 shows the apparent surface pressure−compression area (Π−A) isotherms for nf-CNTs at the air−water interface as a function of successive compression cycles. The surface pressure is termed as "apparent" to indicate that the value obtained from Wilhelmy plates contain both thermodynamic and mechanical contributions as pointed out in a recent paper by Verwijlen et al.[36] Mechanical contribution due to the formation of a CNT network at the interface influences the surface pressure measurements using a Wilhelmy microbalance as force is transmitted through the network during compression. Experimentally, 0.6624 mg of nf-CNT was initially added to the air−water interface. During the first compression, the apparent surface pressure started to rise at 130 cm^2, reaching a maximum value of 63 mN/m as the trough was fully compressed to 23 cm^2. The initial rise of surface pressure is associated with the mechanical percolation of CNTs adsorbed at the interface. In general, surface pressure readings during the first compression may depend on the choice of dispersant and the exact spreading procedure, which influences the initial distribution of particles or molecules and the corresponding microstructure.[37] Following the same spreading protocol, the experiments were repeated twice to check the reproducibility of the experimental data. The surface pressure data of the first compression cycle differed by less than 3.3%. In terms of microstructure, Figure 2a−c shows the corresponding optical texture of the nf-CNT-decorated interface at different stages of compression. The nf-CNTs formed discernible "islands," comprising of dark and gray pixels. The detailed structures of these islands were below the detection threshold of the diffraction-limited optical microscope. To investigate the difference between the dark and gray pixels within the islands, bright-field optical microscopy and scanning electron microscopy were performed on the same sample prepared by Langmuir−Schaefer deposition. A scratch was deliberately placed onto the deposited film, and the same area was imaged. Figure 3 clearly shows the large dark regions corresponding to 3D aggregates.

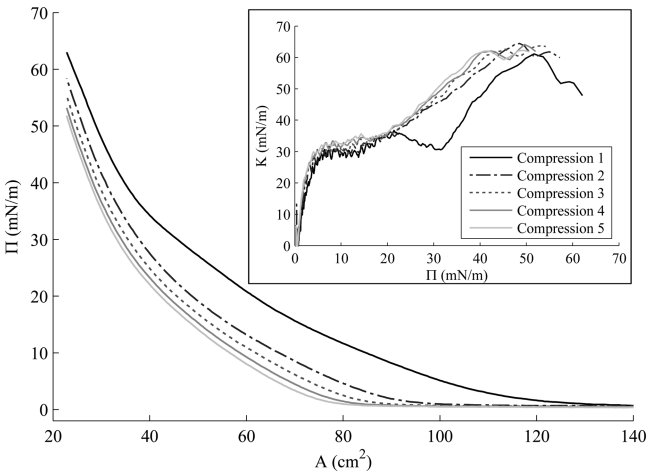

Figure 1. Apparent surface pressure−compression area (Π−A) isotherms of the nf-CNTs (0.6624 mg) for five successive compression cycles at a rate of 5 mm/min. Inset: Compressional elastic modulus (K) as a function of apparent surface pressure (Π) for five compression cycles of nf-CNTs. Temperature = 25 °C.

As shown in Figure 1, for a given trough area, the measured surface pressure decreased progressively in subsequent compression cycles. The largest difference in surface pressure was observed between the first and the second compression cycle, and the difference decreased in successive cycles. The point of percolation, or the compression area at which the surface pressure began to rise, shifts to the left, implying that the network percolates at smaller areas in successive compressions. This is probably due to the loss of CNTs from the interface through CNT desorption and/or 3D aggregation during compression. To study possible CNT desorption, the water subphase was collected, and the corresponding optical absorbance was measured after multiple compression and expansion cycles. Absorbance spectroscopy is capable of detecting the presence of CNTs down to the ppm-level. The water subphase showed no characteristic absorbance of CNTs at 500 nm, ruling out any CNT desorption as in the case of micron-sized particles.[22] Further, Figure 4a−c show the optical micrographs of five compression cycles at a constant trough area of 61 cm^2. To estimate the coverage of 3D CNT aggregates for each compression cycle, the number of dark pixels was normalized by the total number of dark and gray pixels for a given trough area and then averaged for all the trough areas between 243 and 40 cm^2 before wrinkling occurs. As shown in Figure 4d, the aggregate coverage increases as a function of increasing compression cycles, with the largest difference observed between the first and second compression cycle. This is consistent with surface pressure data, where decrease in surface pressure reduces in successive compression cycles for a given trough area (Figure 1). The decrease of surface pressure is associated with the formation of CNT aggregates during compression. Physically, CNT aggregation reduces the area replaced by CNTs, leading to a lower apparent surface pressure and a delayed onset of percolation.

DOI: 10.1021/la504934x
Langmuir 2015, 31, 4663−4672

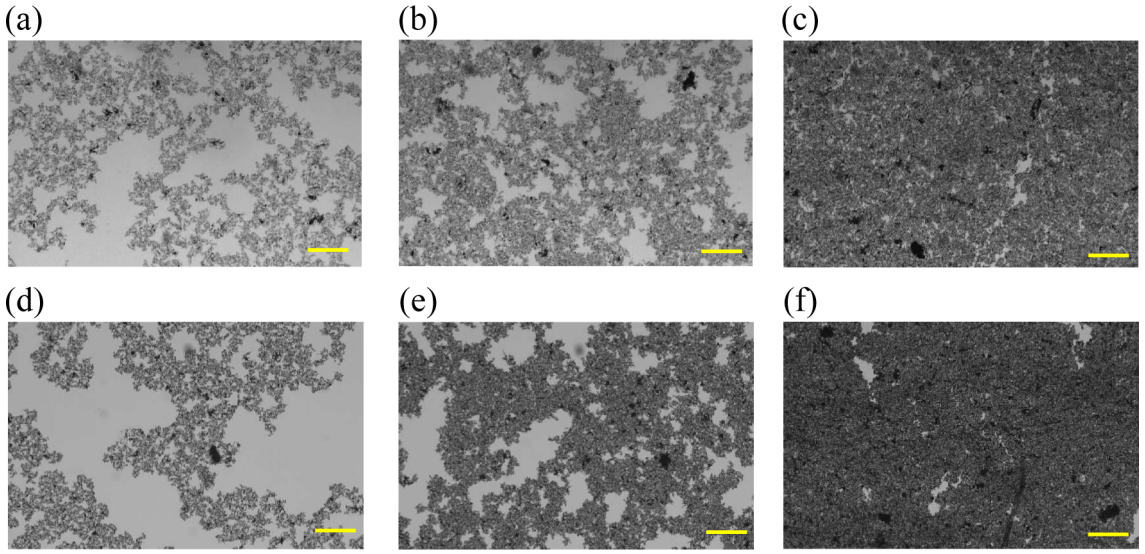

Figure 2. Panels a–c are the optical micrographs during the first compression cycle of nf-CNTs at a trough area of 132 cm^2, 72 cm^2, and 25 cm^2, respectively. Likewise, panels d–f are optical micrographs during the first compression cycle of the f-CNTs at the same trough areas. Scale bar = 100 μm. The compression direction is horizontal in all optical micrographs.

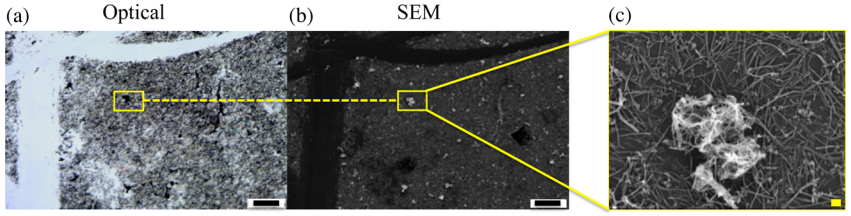

Figure 3. nf-CNT layer was transferred onto a glass slide using the Langmuir–Schaefer deposition. The same area was imaged using optical (a) and electron microscopy (b–c). These images confirmed that the dark pixels observed in optical micrographs correspond to the 3D aggregates. Scale bars: 50 μm in panels a and b; 1 μm in panel c.

On the basis of the surface pressure data, the compressional elastic modulus K of the nf-CNT layer was estimated using eq 1 below.[30]

$$K = -A\frac{\partial \Pi}{\partial A} \tag{1}$$

where A is the trough area, and Π is the surface pressure.

The inset in Figure 1 shows the estimated compressional modulus as a function of surface pressure for five compression cycles. The compressional moduli showed similar values in the second to the fifth compression cycles. The difference between the first and the subsequent cycles was probably caused by some irreversible changes (e.g., aggregation) during the first compression cycle. Interestingly, all cycles showed a plateau between a surface pressure of 5 to 20 mN/m, and a maximum modulus of 60 mN/m was reached at a surface pressure close to 50 mN/m. The initial rise in modulus was probably a result of the densification of CNT islands at the interface. As the CNT islands formed a percolating network, local rotation of some of these islands was observed (see sample video in Supporting Information). The compressional modulus increased again as further rearrangements of islands became impossible, leading to the densification of CNTs within the islands and subsequently the onset of wrinkling similar to those reported in tiled GO sheets.[23]

Functionalized vs Nonfunctionalized CNTs. In the case of functionalized CNT (f-CNT), carboxyl groups (−COOH) were covalently grafted onto CNTs. Lactonic and phenolic groups may also be present.[25] The deprotonation of carboxyl groups in water led to the formation of carboxylate anions, rendering the CNTs negatively charged. The negative charge of f-CNTs was confirmed by measuring the zeta potential of f-CNT in water, which gave a value of −51.4 mV. It should, however, be noted that such analysis did not consider the nonspherical shape and orientation of CNTs relative to the electric field during the measurement. The calculated value was based on the electrophoretic mobility of a sphere with an equivalent hydrodynamic diameter. The addition of −COOH groups also increased the hydrophilicity of the CNTs and reduced the contact angle of CNTs.[38−40] Measuring the contact angle of submicron particles proved to be difficult given their small size.[3] We adopted the "gel trapping" method proposed by Paunov[35] to investigate the contact angle of f-CNTs and nf-CNTs in water. In Paunov's original method, SEM was used, but performing SEM on a nonconductive polydimethylsiloxane (PDMS) sample with sparsely dispersed CNT necessitated the sputtering of a conductive coating. For CNTs with a diameter of ca. 110 nm, the conductive coating masked the CNT features and modified the observed contact angle. For these reasons, AFM instead of SEM was used. Figure 5a and b show two representative AFM images of nf-CNT and f-CNT embedded in the PDMS, respectively. As the PDMS was poured on top of a gelled water subphase to capture the CNTs, the images represent the protrusion of CNT into the water subphase (as shown in the schematic diagrams). A smaller contact angle was observed for f-CNT compared to nf-CNT, as expected for

DOI: 10.1021/la504934x
Langmuir 2015, 31, 4663−4672

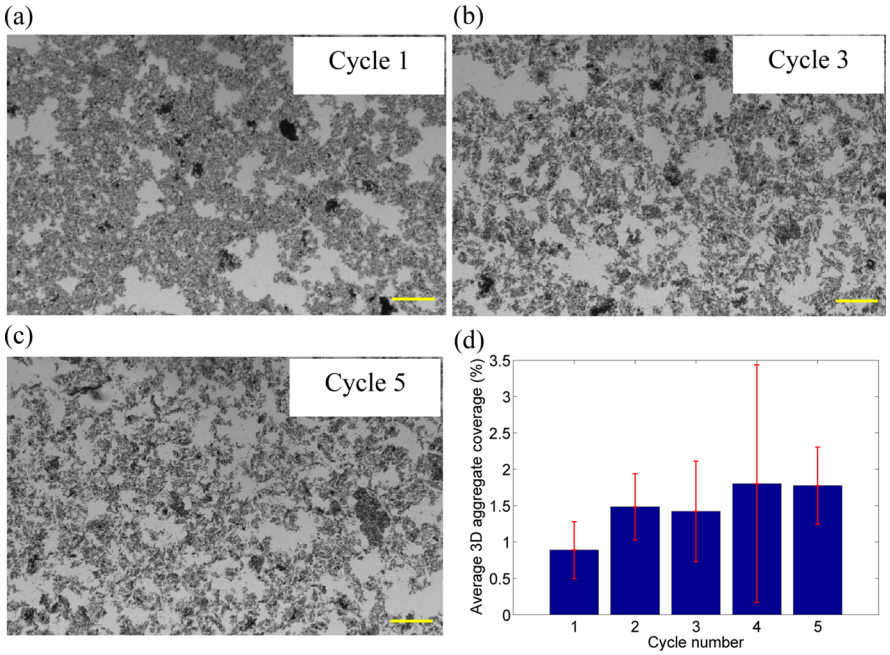

Figure 4. In-situ optical micrographs of the nf-CNTs at the same compression area (61 cm^2) for the first, third, and fifth compression cycles. Panel d shows the average 3D aggregate coverage (%), and the error bar represents the standard deviation based on four independent experiments. The relatively large error bar may be explained by the movement of islands into and out of the rather limited field of view (2.8 mm × 2 mm). For a given trough area, the aggregate coverage is defined as the number of dark pixels (gray scale: 0−50) normalized by the total number of dark and gray pixels (gray scale: 0−155). The average coverage for each cycle is the first moment (mean) of aggregate coverage for trough areas between 243 and 40 cm^2 before the onset of wrinkling. A gray scale corresponding to 8 bits per sampled pixel (256 different intensities) was used for the analysis. The compression direction is horizontal in the optical micrographs. Scale bars in panels a−c: 100 μm.

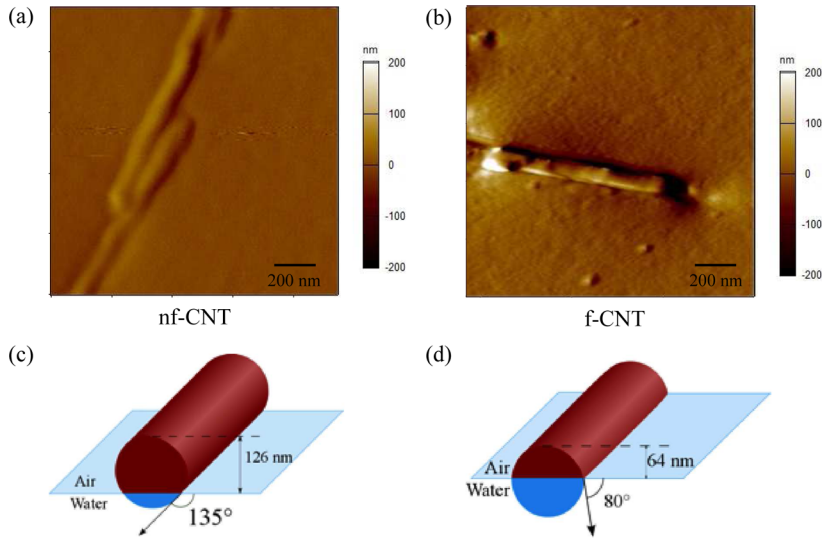

Figure 5. Atomic force microscopy (AFM) images of (a) nf-CNTand (b) f-CNT embedded in polydimethylsiloxane (PDMS), prepared using the gel trapping technique.[35] Schematic diagrams (c and d) show the respective nf-CNT and f-CNT positions at the air−water interface.

particles with higher hydrophilicity. Although no change in surface tension was detected after the addition of gellan gum into water, the position may have shifted during the gelation process. The gel trapping method only serves as a qualitative comparison between the f-CNTs and nf-CNTs.

Previous studies suggested graphitic materials are intrinsically hydrophilic, but their high surface energy lead to the adsorption of hydrocarbons from the ambient environment, resulting in the apparent hydrophobicity.[41,42] The nf-CNTs used in this study have not been purified, and the same may be true, but measuring the intrinsic hydrophilicity is beyond the scope of the current article. Compared to nf-CNTs, a larger area was replaced by the f-CNTs at the air−water interface, leading to a lower overall interfacial energy and a higher surface pressure thermodynamically. However, the measured surface pressure contained both thermodynamic and mechanical contributions. The latter depends on the packing of CNTs at the interface.

Figure 6 shows the Π-A data of f-CNT and the nf-CNT for the first compression cycle. The CNT concentration of the spreading solution was carefully calibrated (See Experimental Methods and Figure S4 in Supporting Information). Optically, f-CNTs absorbed more visible light than nf-CNT, but like nf-

DOI: 10.1021/la504934x
Langmuir 2015, 31, 4663−4672

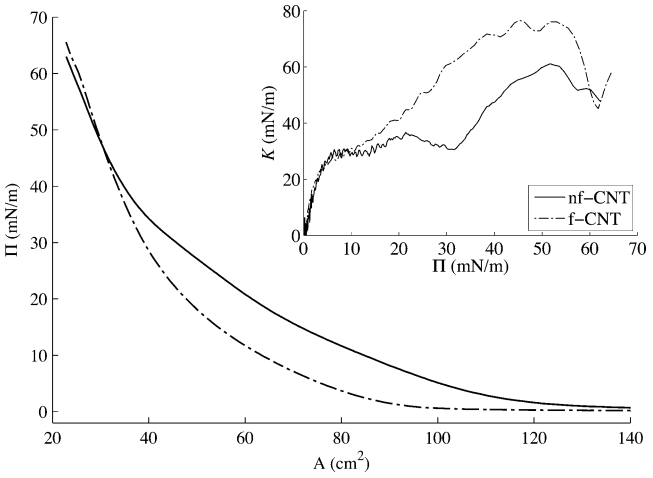

Figure 6. Apparent surface pressure–compression area isotherms for the first compression cycle of nf-CNT and f-CNT (0.6624 mg). The inset figure shows the evolution of compressional elastic modulus as a function of the apparent surface pressure.

CNTs, islands comprising dark and gray pixels were observed (Figure 2d–f). For the same initial amount of CNT, the measured surface pressure of f-CNT began to rise at a smaller trough area. The current article focuses on the compressional behavior of CNTs at an interface, but nf-CNTs and f-CNTs showed strikingly different optical microstructure during the expansion cycles. Representative images are included in the Supporting Information (Figure S7). Detailed length characterization revealed that both nf-CNTs and f-CNTs have similar length distribution. The delayed onset of percolation in the f-CNT case is likely to be caused by the denser packing of CNTs within the islands. Another possible difference between f-CNT and nf-CNT is their flexibility. Previous studies showed that CNTs are semiflexible filaments[43,44] and that covalent functionalization introduces defects onto the CNT sidewalls, possibly lowering the persistence length of the CNTs. However, no noticeable change in the curvature of CNTs was observed in SEM after functionalization. Langmuir–Schaefer deposition was used to characterize the local organization of f-CNT at the interface. Like nf-CNTs, 3D aggregates were present, but pockets of aligned f-CNTs were also observed as shown in Figure 7a and b. SEM micrographs of nf-CNTs and f-CNTs were further analyzed to calculate the fractional coverage of ordered domains (i.e., aligned CNTs), disordered domains (including randomly oriented CNTs and impurities), and voids (Figure 7c). For the same trough area and initial amount added, f-CNTs showed both a higher degree of alignment and denser packing.

Intuitively, the negative charges of f-CNTs induced electrostatic interactions, which further hindered the formation of 3D aggregates and prevented the CNTs from becoming kinetically trapped in the aggregate state, which depends on the interaction potential between CNTs as well as the rate of compression (Figure S6 of Supporting Information). Detailed studies on the effect of compression rate and mechanical modeling will be reported in a future article. Compared with nf-CNTs, f-CNTs were less prone to aggregation (see also Modeling). Although the initial amount of CNT spread onto the interface was the same, the actual coverage was higher in the case of f-CNT for the same trough area. The higher coverage of CNT led to the formation of aligned domains due

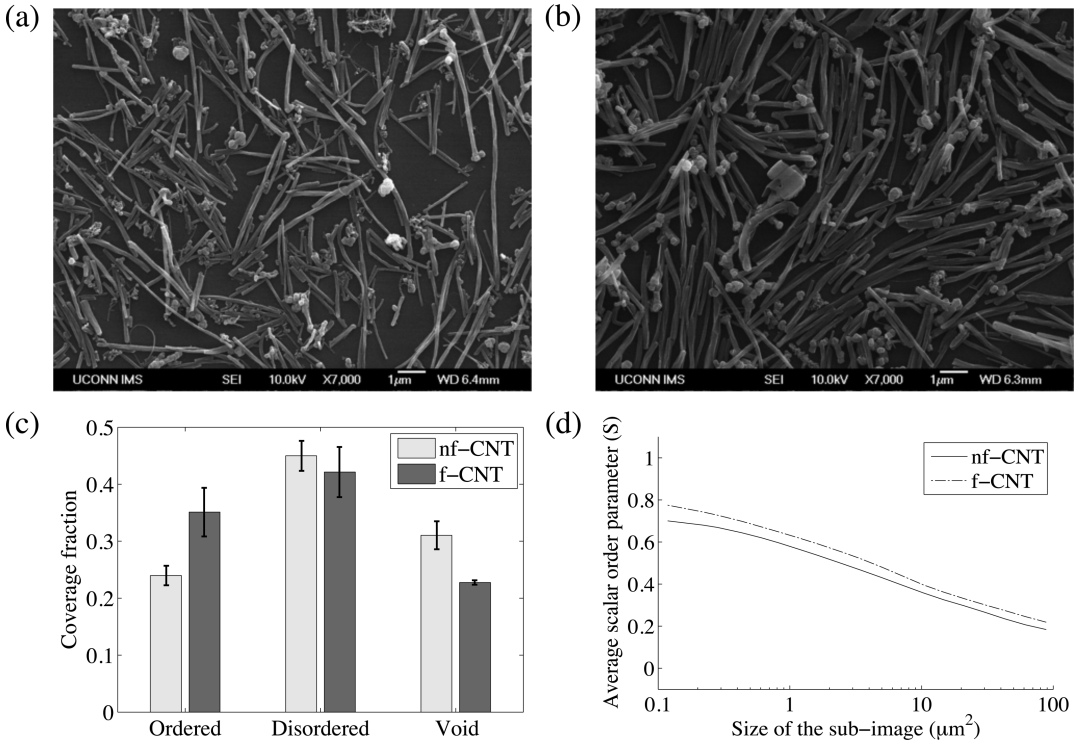

Figure 7. Scanning electron micrographs of (a) nf-CNT and (b) f-CNT layers transferred onto a glass substrate by Langmuir–Schaefer deposition at a trough area of 30 cm^2. A thin layer of gold and palladium (3–5 nm) was sputtered before imaging. Panel c shows the fractional coverage of ordered (aligned CNTs), disordered domains (randomly orientated CNTs and impurities), and voids. Each error bar represents the standard deviation based on four cropped images. Panel d shows the corresponding 2-D scalar order parameter (S) for nf-CNTs and f-CNTs calculated from the micrographs.

DOI: 10.1021/la504934x
Langmuir 2015, 31, 4663–4672

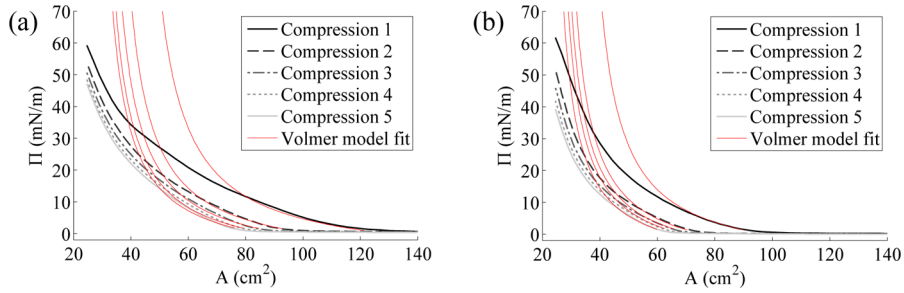

Figure 8. Volmer model fits (red lines) to the experimental data of (a) nf-CNTs and (b) f-CNTs for five compression cycles. The values for the fitting parameters obtained are tabulated in Table 1.

to excluded volume interactions, as in the case of liquid crystals. To quantify the degree of alignment in each case, the concept of scalar order parameter was borrowed from the liquid crystal literature. Figure 7d shows the corresponding 2-D scalar order parameter (S) for nf-CNTs and f-CNTs calculated from the SEM micrographs. A S value of "1" indicates the CNTs within the area of interest are fully aligned, whereas a value of "0" indicates completely randomly oriented CNTs. The actual S value depends on the area of interest and should reach a value of 1 as the area approaches that of a single CNT.[45] As shown in Figure 7d, f-CNTs showed a consistently higher S value compared with that of nf-CNTs.

Liquid crystals have been reported for oxidized CNTs suspended in water[27,46,47] and pristine CNTs in superacids.[48] However, the physics is more complicated for CNTs at an interface because of the presence of dipolar interactions, due to the asymmetric distribution of counterions on the air and water sides, and lateral capillary interactions.[21,49] Kim et al.[50] reported the formation of raft-like aggregates, 2D nematic, 2D smectic, and 3D nematic phases for nanorods compressed at the air−water interface. The inset of Figure 6 compares the compressional modulus of nf-CNT and that of f-CNT estimated from surface pressure data. f-CNTs formed a stiffer layer compared to nf-CNTs at the interface, which may be explained by the formation of aligned CNT domains and denser packing.

Modeling Surface Pressure Data. Volmer equation of state (eq 2) was used to model the surface pressure data of both nf-CNTs and f-CNTs. This model has been successfully applied to describe the surface pressure data of micro- and nanoparticles[33] and more recently GO.[23]

$$\Pi = \frac{kT\left(\frac{\omega}{A}\right)}{\omega_o\left(1 - \frac{\omega}{A}\right)} - \Pi_{coh} \tag{2}$$

where k is the Boltzmann constant, and T is the absolute temperature.

In the Volmer model, there are two fitting parameters, namely, the area replaced by the particles (ω) and the cohesion pressure (Π_{coh}), although many studies also used the molecular area of a solvent molecule (ω_o) as the third fitting parameter.[33] In this article, ω_o is chosen to be 0.2 nm^2 (theoretical value for water) to avoid the use of unrealistic values for data fitting. Figure 8 shows the Volmer model fits to the experimental data of nf-CNTs and f-CNTs for five compression cycles. For each type of CNTs, a single value of Π_{coh} was used for all of the compression cycles. Π_{coh} is a lumped parameter accounting for CNT−CNT interactions and CNT−solvent interactions, but no explicit expression is readily available. For each compression cycle, ω was held constant (i.e., independent of the trough area), but the value of ω was allowed to vary from cycle to cycle. From the data fit values in Table 1, ω decreased as a function of compression cycles, which is consistent with the experimental observations of 3D aggregation. For 0.63 mg of CNT added onto the surface, if we assume an average diameter of 110 nm and an average density of 1.5 g/cm^3 for the CNTs, the initial coverage is estimated to be ca. 36 cm^2 calculated using eqs 3 and 4:

Table 1. Volmer Model Fitting Parameters for the Plots in Figure 8[a]

type of CNT	ω_1 (cm^2)	ω_2 (cm^2)	ω_3 (cm^2)	ω_4 (cm^2)	ω_5 (cm^2)	Π_{coh} (mN/m)
nf-CNT	40.44	32.07	29.39	27.65	26.72	9.32
f-CNT	32.48	25.42	24.11	23.11	21.85	10.27

[a] ω_o is the molecular area of a water molecule and has a constant value of 0.2 nm^2.

$$m = N\rho\pi r^2 L \tag{3}$$

where m is the mass of CNTs, N is the number of CNTs, ρ is the density of the CNTs, r is the radius, and L is the length of the CNTs.

$$\omega = 2Nr\sin\theta L = \frac{2m\sin\theta}{\rho\pi r} \tag{4}$$

where θ is the contact angle of the CNT.

From the model fits, the initial coverages (ω_1) are 40.44 cm^2 and 32.48 cm^2 for nf-CNT and f-CNT, respectively. Despite the polydispersity of CNT in terms of diameter, length, and density, these values are reasonably close to the value estimated from the CNT diameter and density. From the fits, Π_{coh} is determined to be 9.32 and 10.27 mN/m for nf-CNTs and f-CNTs, respectively. These values are comparable to those reported by Imperiali et al.[23] for GO.

However, as shown in Figure 8, the Volmer model overpredicted the surface pressure at high coverage in both cases. Experimentally, 3D aggregation of CNTs was observed for both nf-CNTs and f-CNTs during the compression cycles. The implication is a reduction in actual area replaced by CNTs, and a smaller ω value. If we allow ω to vary as a function of trough area, the actual coverage of CNTs during each compression cycles can be deduced (Figure 9a and b). At small trough areas, nf-CNTs showed a larger slope (Figure 9a) and hence a larger loss of interfacial coverage due to 3D aggregation compared with that of f-CNTs (Figure 9b). This is in agreement with the physical picture that f-CNTs are less prone to aggregation due to additional electrostatic interactions between f-CNTs. Figure 9c shows the normalized interfacial

DOI: 10.1021/la504934x
Langmuir 2015, 31, 4663−4672

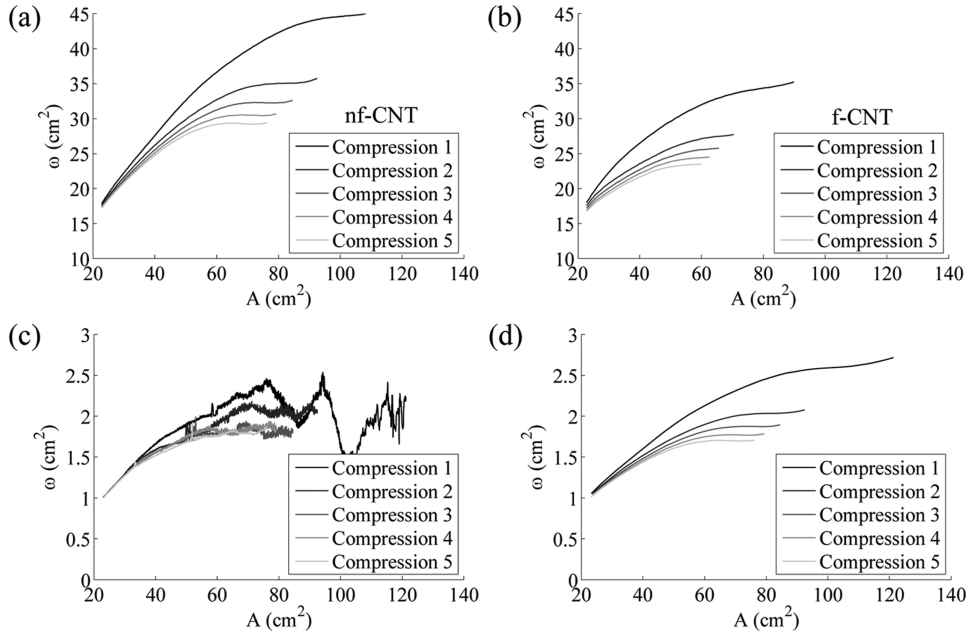

Figure 9. (a and b) CNT interfacial coverage (ω) back calculated from Volmer model fits for five compression cycles, where ω was allowed to vary as a function of compression area (A). Panel c shows the normalized nf-CNT coverage (ω) estimated experimentally from the optical micrographs. (d) Normalized ω deduced from the Volmer model fits. Initial amount of nf-CNT: 0.6624 mg.

coverage estimated from counting the total number of dark and gray pixels in the optical images, and Figure 9d shows the interfacial coverage deduced from the model fit. The variation of ω determined from optical images, especially significant at large trough areas, is caused by the motion of CNT islands and the limited field of view of the optical micrographs. However, reasonable agreement between the CNT coverage determined from the model fit and that from optical images was observed. The experimentally determined coverage for compression cycles 3−5 is slightly higher than that estimated from the Volmer model. The overestimation of CNT coverage is probably due to the presence of voids within the CNT islands. In estimating the experimental ω value, no distinction was made between the dark and gray pixels, and the CNT islands were assumed to be completely covered by CNTs.

CONCLUSIONS

The apparent surface pressure and corresponding microstructure of two different types of CNTs at an air−water interface were reported. They were as-produced CNTs (nf-CNTs) and CNTs functionalized with carboxyl groups (f-CNTs). Both nf-CNTs and f-CNTs had a similar length distribution, but f-CNTs were more hydrophilic, confirmed by a modified gel trapping method. Upon compression, both types of CNTs showed some degree of 3D aggregation, manifested as dark pixels in the optical images. However, no desorption of CNTs from the interface was detected by absorbance spectroscopy. nf-CNTs showed a higher aggregation propensity compared with that of f-CNTs. This was attributed to the formation of carboxylate anions and consequently electrostatic repulsions in the case of f-CNTs. For the same initial coverage, f-CNTs showed a higher degree of orientational ordering upon compression relative to nf-CNTs. The orientational ordering was probably caused by the excluded volume interactions, analogous to the formation of liquid crystals in 3D. In terms of compressional elastic modulus, both nf-CNTs and f-CNTs displayed a maximum value at a surface pressure close to 50 mN/m. However, the f-CNT-decorated interface was about 28% stiffer than the nf-CNT-decorated interface. This is attributable to lower degree of 3D aggregation and as a result higher actual coverage and denser packing in the f-CNT case. Finally, Volmer equation of state was used to model the measured surface pressure containing both thermodynamic and mechanical contributions. The Volmer model assumed a constant interfacial coverage (ω) for each cycle and over-predicted the surface pressure at large compression. Instead of keeping ω constant for each compression cycle, the Volmer model was used to back calculate the actual CNT coverage during compression and the loss of CNTs due to 3D aggregation. The coverage estimated from the Volmer model was consistent with the coverage estimated from the optical images.

To summarize, all existing studies on particles at an interface focus on 2D aggregation.[16,32,50] This work is one of the first studies showing simultaneous 3D aggregation and 2D orientational ordering of rod-like particles with high aspect ratios (>40) at an air−water interface. The observed 3D aggregation may be related to and yet different from the "flipping" of ellipsoid particles with a modest aspect ratio (<10).[22] A new modified Volmer model involving the use of a variable surface coverage (ω) is proposed and justified. Such a model and fundamental understanding may be extended to other systems involving rod-like particles with a high aspect ratio at an air−water interface.

ASSOCIATED CONTENT

Supporting Information

Video showing first compression cycle of nf-CNT; Raman spectra of nf-CNT and f-CNT; length and diameter distribution; calibration curves for calculating the CNT concentration in spreading dispersions; surface pressure−compression area isotherms with platinum and paper Wilhelmy plates; surface pressure−compression area isotherms at different rates of compression; and micrographs of nf-CNT and f-

DOI: 10.1021/la504934x
Langmuir 2015, 31, 4663−4672

CNT during expansion. This material is available free of charge via the Internet at http://pubs.acs.org.

AUTHOR INFORMATION

Corresponding Author

*E-mail: anson.ma@uconn.edu.

Notes

Any opinion, findings, and conclusions or recommendations expressed in this material are those of the authors(s) and do not necessarily reflect the views of the National Science Foundation.

The authors declare no competing financial interest.

ACKNOWLEDGMENTS

We thank Professor H. Henning Winter (UMass Amherst) for helpful discussions. This material is based upon work supported by the U.S. National Science Foundation CAREER award under grant no. 1253613.

REFERENCES

(1) Ramsden, W. Separation of Solids in the Surface-Layers of Solutions and "Suspensions" (Observations on Surface-Membranes, Bubbles, Emulsions, and Mechanical Coagulation). Preliminary Account. *Proc. R. Soc. London* **1903**, *72*, 156−164.

(2) Pickering, S. U. CXCVI. Emulsions. *J. Chem. Soc. Trans.* **1907**, *91*, 2001.

(3) Binks, B. P. Particles as Surfactants—Similarities and Differences. *Curr. Opin. Colloid Interface Sci.* **2002**, *7*, 21−41.

(4) Lin, Y.; Skaff, H.; Emrick, T.; Dinsmore, A. D.; Russell, T. P. Nanoparticle Assembly and Transport at Liquid-Liquid Interfaces. *Science* **2003**, *299*, 226−229.

(5) Yoon, K. Y.; An, S. J.; Chen, Y.; Lee, J. H.; Bryant, S. L.; Ruoff, R. S.; Huh, C.; Johnston, K. P. Graphene Oxide Nanoplatelet Dispersions in Concentrated NaCl and Stabilization of Oil/Water Emulsions. *J. Colloid Interface Sci.* **2013**, *403*, 1−6.

(6) Worthen, A. J.; Bagaria, H. G.; Chen, Y.; Bryant, S. L.; Huh, C.; Johnston, K. P. Nanoparticle-Stabilized Carbon Dioxide-in-Water Foams with Fine Texture. *J. Colloid Interface Sci.* **2013**, *391*, 142−151.

(7) Venkataraman, P.; Tang, J.; Frenkel, E.; McPherson, G. L.; He, J.; Raghavan, S. R.; Kolesnichenko, V.; Bose, A.; John, V. T. Attachment of a Hydrophobically Modified Biopolymer at the Oil-Water Interface in the Treatment of Oil Spills. *ACS Appl. Mater. Interfaces* **2013**, *5*, 3572−3580.

(8) Gupta, A.; Sender, M.; Fields, S.; Bothun, G. D. Phase and Sedimentation Behavior of Oil (octane) Dispersions in the Presence of Model Mineral Aggregates. *Mar. Pollut. Bull.* **2014**, *87*, 164−170.

(9) Pieranski, P. Two-Dimensional Interfacial Colloidal Crystals. *Phys. Rev. Lett.* **1980**, *45*, 569−572.

(10) Hurd, A. J. The Electrostatic Interaction between Interfacial Colloidal Particles. *J. Phys. A: Math. Gen.* **1985**, *18*, L1055−L1060.

(11) Park, B. J.; Pantina, J. P.; Furst, E. M.; Oettel, M.; Reynaert, S.; Vermant, J. Direct Measurements of the Effects of Salt and Surfactant on Interaction Forces between Colloidal Particles at Water-Oil Interfaces. *Langmuir* **2008**, *24*, 1686−1694.

(12) Masschaele, K.; Park, B. J.; Furst, E. M.; Fransaer, J.; Vermant, J. Finite Ion-Size Effects Dominate the Interaction between Charged Colloidal Particles at an Oil-Water Interface. *Phys. Rev. Lett.* **2010**, *105*, 048303.

(13) Nikolaides, M. G.; Bausch, A. R.; Hsu, M. F.; Dinsmore, A. D.; Brenner, M. P.; Gay, C.; Weitz, D. A. Electric-Field-Induced Capillary Attraction between like-Charged Particles at Liquid Interfaces. *Nature* **2002**, *420*, 299−301.

(14) Megens, M.; Aizenberg, J. Capillary Attraction: Like-Charged Particles at Liquid Interfaces. *Nature* **2003**, *424*, 1014 discussion 1014..

(15) Kralchevsky, P. A.; Nagayama, K. *Particles at Fluid Interfaces and Membranes*; Elsevier: New York, 2001; Vol. *10*.

(16) Cavallaro, M.; Botto, L.; Lewandowski, E. P.; Wang, M.; Stebe, K. J. Curvature-Driven Capillary Migration and Assembly of Rod-like Particles. *Proc. Natl. Acad. Sci. U.S.A.* **2011**, *108*, 20923−20928.

(17) van Nierop, E. A.; Stijnman, M. A.; Hilgenfeldt, S. Shape-Induced Capillary Interactions of Colloidal Particles. *Europhys. Lett.* **2005**, *72*, 671−677.

(18) Stamou, D.; Duschl, C.; Johannsmann, D. Long-Range Attraction between Colloidal Spheres at the Air-Water Interface: The Consequence of an Irregular Meniscus. *Phys. Rev. E* **2000**, *62*, 5263−5272.

(19) Danov, K. D.; Kralchevsky, P. A.; Boneva, M. P. Electrodipping Force Acting on Solid Particles at a Fluid Interface. *Langmuir* **2004**, *20*, 6139−6151.

(20) Lehle, H.; Noruzifar, E.; Oettel, M. Ellipsoidal Particles at Fluid Interfaces. *Eur. Phys. J. E: Soft Matter Biol. Phys.* **2008**, *26*, 151−160.

(21) Botto, L.; Lewandowski, E. P.; Cavallaro, M.; Stebe, K. J. Capillary Interactions between Anisotropic Particles. *Soft Matter* **2012**, *8*, 9957.

(22) Basavaraj, M.; Fuller, G.; Fransaer, J.; Vermant, J. Packing, Flipping, and Buckling Transitions in Compressed Monolayers of Ellipsoidal Latex Particles. *Langmuir* **2006**, *22*, 6605−6612.

(23) Imperiali, L.; Liao, K.-H.; Clasen, C.; Fransaer, J.; Macosko, C. W.; Vermant, J. Interfacial Rheology and Structure of Tiled Graphene Oxide Sheets. *Langmuir* **2012**, *28*, 7990−8000.

(24) Cui, M.; Emrick, T.; Russell, T. P. Stabilizing Liquid Drops in Nonequilibrium Shapes by the Interfacial Jamming of Nanoparticles. *Science* **2013**, *342*, 460−463.

(25) Feng, T.; Hoagland, D. A.; Russell, T. P. Assembly of Acid-Functionalized Single-Walled Carbon Nanotubes at Oil/water Interfaces. *Langmuir* **2014**, *30*, 1072−1079.

(26) Liu, J.; Rinzler, A. G.; Dai, H.; Hafner, J. H.; Bradley, R. K.; Boul, P. J.; Lu, A.; Iverson, T.; Shelimov, K.; Huffman, C. B.; et al. Fullerene Pipes. *Science* **1998**, *280*, 1253−1256.

(27) Song, W.; Windle, A. H. Isotropic−Nematic Phase Transition of Dispersions of Multiwall Carbon Nanotubes. *Macromolecules* **2005**, *38*, 6181−6188.

(28) Osswald, S.; Havel, M.; Gogotsi, Y. Monitoring Oxidation of Multiwalled Carbon Nanotubes by Raman Spectroscopy. *J. Raman Spectrosc.* **2007**, *38*, 728−736.

(29) Russell, J. M.; Oh, S.; LaRue, I.; Zhou, O.; Samulski, E. T. Alignment of Nematic Liquid Crystals Using Carbon Nanotube Films. *Thin Solid Films* **2006**, *509*, 53−57.

(30) Cicuta, P.; Terentjev, E. M. Viscoelasticity of a Protein Monolayer from Anisotropic Surface Pressure Measurements. *Eur. Phys. J. E: Soft Matter Biol. Phys.* **2005**, *16*, 147−158.

(31) Petkov, J. T.; Gurkov, T. D.; Campbell, B. E.; Borwankar, R. P. Dilatational and Shear Elasticity of Gel-like Protein Layers on Air/Water Interface. *Langmuir* **2000**, *16*, 3703−3711.

(32) Reynaert, S.; Moldenaers, P.; Vermant, J. Control over Colloidal Aggregation in Monolayers of Latex Particles at the Oil-Water Interface. *Langmuir* **2006**, *22*, 4936−4945.

(33) Fainerman, V. B.; Kovalchuk, V. I.; Lucassen-Reynders, E. H.; Grigoriev, D. O.; Ferri, J. K.; Leser, M. E.; Michel, M.; Miller, R.; Möhwald, H. Surface-Pressure Isotherms of Monolayers Formed by Microsize and Nanosize Particles. *Langmuir* **2006**, *22*, 1701−1705.

(34) Monteux, C.; Kirkwood, J.; Xu, H.; Jung, E.; Fuller, G. G. Determining the Mechanical Response of Particle-Laden Fluid Interfaces Using Surface Pressure Isotherms and Bulk Pressure Measurements of Droplets. *Phys. Chem. Chem. Phys.* **2007**, *9*, 6344−6350.

(35) Paunov, V. Novel Method for Determining the Three-Phase Contact Angle of Colloid Particles Adsorbed at Air-Water and Oil-Water Interfaces. *Langmuir* **2003**, *19*, 7970−7976.

(36) Verwijlen, T.; Imperiali, L.; Vermant, J. Separating Viscoelastic and Compressibility Contributions in Pressure-Area Isotherm Measurements. *Adv. Colloid Interface Sci.* **2014**, *206*, 428−436.

(37) Duncan, S. L.; Larson, R. G. Comparing Experimental and Simulated Pressure-Area Isotherms for DPPC. *Biophys. J.* **2008**, *94*, 2965−2986.

DOI: 10.1021/la504934x
Langmuir 2015, 31, 4663−4672

(38) Menzel, R.; Lee, A.; Bismarck, A.; Shaffer, M. S. P. Inverse Gas Chromatography of as-Received and Modified Carbon Nanotubes. *Langmuir* **2009**, *25*, 8340−8348.
(39) Menzel, R.; Bismarck, A.; Shaffer, M. S. P. Deconvolution of the Structural and Chemical Surface Properties of Carbon Nanotubes by Inverse Gas Chromatography. *Carbon* **2012**, *50*, 3416−3421.
(40) Goode, A. E.; Hine, N. D. M.; Chen, S.; Bergin, S. D.; Shaffer, M. S. P.; Ryan, M. P.; Haynes, P. D.; Porter, A. E.; McComb, D. W. Mapping Functional Groups on Oxidised Multi-Walled Carbon Nanotubes at the Nanometre Scale. *Chem. Commun.* **2014**, *50*, 6744−6747.
(41) Kozbial, A.; Li, Z.; Conaway, C.; McGinley, R.; Dhingra, S.; Vahdat, V.; Zhou, F.; D'Urso, B.; Liu, H.; Li, L. Study on the Surface Energy of Graphene by Contact Angle Measurements. *Langmuir* **2014**, *30*, 8598−8606.
(42) Li, Z.; Wang, Y.; Kozbial, A.; Shenoy, G.; Zhou, F.; McGinley, R.; Ireland, P.; Morganstein, B.; Kunkel, A.; Surwade, S. P.; et al. Effect of Airborne Contaminants on the Wettability of Supported Graphene and Graphite. *Nat. Mater.* **2013**, *12*, 925−931.
(43) Fakhri, N.; Tsyboulski, D. A.; Cognet, L.; Weisman, R. B.; Pasquali, M. Diameter-Dependent Bending Dynamics of Single-Walled Carbon Nanotubes in Liquids. *Proc. Natl. Acad. Sci. U.S.A.* **2009**, *106*, 14219−14223.
(44) Pagani, G.; Green, M. J.; Poulin, P.; Pasquali, M. Competing Mechanisms and Scaling Laws for Carbon Nanotube Scission by Ultrasonication. *Proc. Natl. Acad. Sci. U.S.A.* **2012**, *109*, 11599−11604.
(45) Shaffer, M.; Fan, X.; Windle, A. Dispersion and Packing of Carbon Nanotubes. *Carbon* **1998**, *36*, 1603−1612.
(46) Song, W.; Kinloch, I. A.; Windle, A. H. Nematic Liquid Crystallinity of Multiwall Carbon Nanotubes. *Science* **2003**, *302*, 1363.
(47) Song, W.; Windle, A. H. Size-Dependence and Elasticity of Liquid-Crystalline Multiwalled Carbon Nanotubes. *Adv. Mater.* **2008**, *20*, 3149−3154.
(48) Davis, V. A.; Ericson, L. M.; Parra-Vasquez, A. N. G.; Fan, H.; Wang, Y.; Prieto, V.; Longoria, J. A.; Ramesh, S.; Saini, R. K.; Kittrell, C.; et al. Phase Behavior and Rheology of SWNTs in Superacids. *Macromolecules* **2004**, *37*, 154−160.
(49) Wolfe, D. B.; Snead, A.; Mao, C.; Bowden, N. B.; Whitesides, G. M. Mesoscale Self-Assembly: Capillary Interactions When Positive and Negative Menisci Have Similar Amplitudes. *Langmuir* **2003**, *19*, 2206−2214.
(50) Kim, F.; Kwan, S.; Akana, J.; Yang, P. Langmuir-Blodgett Nanorod Assembly. *J. Am. Chem. Soc.* **2001**, *123*, 4360−4361.

DOI: 10.1021/la504934x
Langmuir 2015, 31, 4663−4672